Available online at www.sciencedirect.com
SCIENCE DIRECT
Polymer 47 (2006) 5445–5456
polymer
www.elsevier.com/locate/polymer

High pressure crystallization of random propylene–ethylene copolymers: α–γ Phase diagram

Anita Dimeska [a,1], Paul J. Phillips [b,*]

[a] Department of Materials Science and Engineering, University of Tennessee, Knoxville, TN, USA
[b] Department of Chemical and Materials Engineering, University of Cincinnati, Cincinnati, OH 45221 0012, USA

Received 14 January 2005; received in revised form 19 November 2005; accepted 23 November 2005
Available online 23 May 2006

Abstract

Two random propylene copolymers with low ethylene content synthesized by Ziegler–Natta catalysts were used is this study to investigate the formation of γ-crystal phase during isothermal crystallization at high pressures. At atmospheric pressure these copolymers crystallize in a mixture of α- and γ-crystals. The content of the γ-phase in the copolymer crystals increased with increasing defect content, crystallization temperature and pressure. Wide-angle X-ray diffraction studies showed that crystallization of these copolymers at pressures above 88 MPa and temperature above 142 °C leads to formation of pure γ-phase. The equilibrium melting temperature of the γ-phase has been determined as a function of defect content and crystallization pressure. Temperature–pressure-composition α–γ phase diagram of isotactic polypropylene was constructed based on the Gibbs free energy approach. This diagram enabled the extrapolation of the equilibrium melting temperatures of both phases for defect free isotactic polypropylene. They were found to be 186.9°C for the α-phase and 189.9°C for the γ-phase.
© 2006 Elsevier Ltd. All rights reserved.

Keywords: α-phase; γ-phase; Phase diagram

1. Introduction

Isotactic polypropylene (*i*-PP) is one of the most important commercial polymers. Since the discovery of Ziegler–Natta catalyst systems and their subsequent industrial application, this polymer has received increasing scientific and commercial attention. It is well known that *i*-PP can exist in three polymorphic crystalline forms, α, β, and γ, that differ in the arrangement and packing of the chains [1–5]. α-Form is the most common crystal form, that is observed for both solution and melt crystallized samples prepared at atmospheric pressure. The metastable β-form is obtained sporadically at high supercoolings or in the presence of selective β nucleating agents.

The γ-form is probably the most interesting among the crystal forms of *i*-PP. It has been shown that several factors can lead to the formation of the γ-form: (i) crystallization under high pressure [6–10], (ii) crystallization of low molecular weight fractions [3,11], (iii) slow cooling from the melt [4], (iv) presence of chain defects or chemical heterogeneity caused by atacticity [12,13], (v) presence of the comonomer units in the chain [14–17], and (vi) melt vibration [18].

In the 1960's, the development of γ-form of *i*-PP crystallized under high pressures was observed for the first time. Kardos et al. [19] reported the formation of γ-form in samples isothermally crystallized, as well as slow cooled from the melt at pressures above 320 atm. With increasing pressure a larger portion of the samples crystallized in the γ-form until 5000 atm where only the γ-form was present. Sauer and Pae [20] investigated the crystal structure, thermal and melting behavior, and the morphology of the pressure-crystallized *i*-PP. For all studied temperatures and pressures the material crystallized into the γ-form, which was stable at low degrees of supercooling. They suggested that for pressure-crystallized samples γ-form was the most stable one, which was also suggested by other authors [19,21]. The rate of $\gamma \rightarrow \alpha$ transformation was found by Pae [22] to be a function of time and temperature. In addition, based on the DSC studies it was concluded that the γ-phase melted without conversion into the α-phase.

Extensive research on the γ form of high molecular weight *i*-PP with high isotacticity crystallized under high pressures was reported by Mezghani and Phillips [9,10]. These studies

* Corresponding author.
E-mail address: paul.phillips@uc.edu (P.J. Phillips).
[1] Present address: Novolen Technology Holdings, Equistar Technology Center, Cincinnati, OH, 45249, USA.

0032-3861/$ - see front matter © 2006 Elsevier Ltd. All rights reserved.
doi:10.1016/j.polymer.2005.11.097

confirmed that the formation of the γ-form is preferred at high pressures and low degrees of supercooling. Additionally, the equilibrium melting temperature and heat of fusion of pure γ form at atmospheric and high pressures were determined. Based on the melting behavior and polymorphism the phase diagram of *i*-PP was constructed, which enabled the thermodynamic prediction of pure γ form as a function of crystallization temperature and pressure.

Even though studies of Ziegler–Natta propylene–ethylene copolymers at atmospheric pressure indicated that a high amount of the γ-phase can be generated [15,23–26], there are no published reports on whether pure γ-phase can be obtained at high pressures. In the present study, the effect of the crystallization pressure on the development of γ-phase in random Ziegler–Natta propylene–ethylene copolymers was investigated. It was shown that, analogous to the *i*-PP homopolymer crystallization, elevated pressures enhanced the formation of the γ-phase crystals. Also, the presence of defects in *i*-PP chains shifted the onset of pure γ-phase formation in these propylene–ethylene copolymers to lower crystallization temperatures. Results from high pressure crystallization of copolymers were used for further expanding the phase diagram of the *i*-PP homopolymer to include the defect content. This temperature–pressure-composition α–γ phase diagram of *i*-PP enabled the extrapolation of the equilibrium melting temperatures of α and γ phases for defect free *i*-PP.

2. Experimental

2.1. Materials

Two copolymer fractions obtained by solution fractionation of two commercial propylene–ethylene copolymers synthesized by Ziegler–Natta catalyst and kindly supplied by ExxonMobil Chemical Company were used. Molecular characterization of the copolymer fractions was carried out by solution ^{13}C nuclear magnetic resonance (NMR) and gel permeation chromatography (GPC). ^{13}C NMR measurements were performed on a Bruker AMX-400 NMR spectrometer at 112 °C. 10% (w/v) polymer solutions were prepared in *o*-dichlorobenzene, with d_6-benzene (DMSO) as an internal lock. Molecular weight data were obtained on Polymer Laboratories PL-GPC 220, equipped with a precision detector PD2040 dual angle (90 and 15°) light scattering detector. Table 1 lists the characteristics of studied copolymer samples, that are labeled according to their mole percentage of ethylene units. They have similar molecular weight and molecular weight distribution. The NMR analysis showed that they have only isolated ethylene and stereo defects, and do not contain regio-defects.

Table 1
Molecular weight characteristics of propylene–ethylene copolymers

Sample ID	Ethylene (mol%)	Stereo (mol%)	Total defects (mol%)	M_w (g/mol)	M_w/M_n
*i*PP2.62	2.62	3.14	5.76	252,200	2.09
*i*PP4.38	4.38	7.22	11.60	287,100	1.98

2.2. Sample preparation

Copolymer polymorphism studies were carried out on thick film samples prepared by isothermal crystallization in a custom piston-cylinder type high pressure cell. A Carver hydraulic press equipped with heated platens was used in this experiment. After the sample was properly mounted into the cell, the cell assembly was placed between the press platens and heated to an appropriate melting temperature for a time sufficient to ensure complete melting, typically 15 min. The cell temperature was then lowered to the desired crystallization temperature. The pressure was applied after the crystallization temperature was stabilized. Sufficient time was provided to ensure complete crystallization of the sample under constant pressure and temperature. Afterwards the temperature of the cell was lowered to room temperature and then the pressure was released. Both copolymer samples were crystallized at four pressures (88, 123, 158 and 193 MPa) and several crystallization temperatures.

2.3. Differential scanning calorimetry (DSC)

The melting behavior of the samples crystallized at high pressures was studied using TA Q1000 V7.3 differential scanning calorimeter. The temperature and heat capacity calibrations were performed with pure metal standards. Pure indium standard was used for temperature calibration, while sapphire standard was used for heat capacity calibration. Samples weighting 6 ± 1 mg enclosed in Al-pans were heated at a scanning rate of 10 °C/min. Melting temperatures were determined from the melting curves as the peak temperatures.

2.4. Wide angle X-ray diffraction (WAXD)

WAXD experiments were performed on a Philips X'Pert plus diffractometer in the reflection mode, with filtered Cu Kα radiation as X-ray source. The patterns were acquired for 2θ range between 5 and 35°, with a step size of 0.03° and scan rate of 0.4 °/min. Peak assignments given by Turner–Jones [27] were used for the α-phase, while assignments given by Bruckner and Meille [28] were used for the γ-phase. The degree of crystallinity of the copolymers was calculated from the relative areas of the amorphous and crystalline peaks. The amount of the γ-form present in the samples was determined from the heights of the (117) Bragg peak of the γ-form at $2\theta = 20.1°$, and the (130) Bragg peak of the α-form at $2\theta = 18.6°$ according to the method given by Turner–Jones [27] as $\gamma = I_{117}/(I_{117} + I_{130})$.

2.5. Small angle X-ray scattering (SAXS)

SAXS pinhole patterns were recorded on a Molecular Metrology SAXS system with sample-to-detector distance of 0.5 and 1.5 m to cover the scattering vector range of $0.07 < q < 5.0\ nm^{-1}$. The X-ray generator was a copper microfocused

X-ray beam, operated at 45 kV and 0.66 mA. Raw scattering data were corrected for background scattering, sample absorption, and thermal density fluctuations. Lamellar thickness of the samples was determined using the self-correlation triangle method of the one-dimensional correlation function [29].

3. Results

3.1. WAXD

WAXD patterns of copolymer *i*PP2.62 crystallized at 88 and 193 MPa as a function of crystallization temperature are shown in Figs. 1 and 2, respectively. The diffractogram of *i*PP2.62 crystallized at the lowest crystallization pressure shows that these samples crystallize into both α- and γ-crystal phases. At this pressure, even at very high crystallization temperatures only a mixture of these phases was produced, as indicated by the presence of the characteristic peaks of both crystal phases. However, for all other studied pressures, 123, 158 and 193 MPa, pure γ-crystal phase was obtained at higher crystallization temperatures, as seen from the absence of the characteristic α-phase (130) reflection shown in Fig. 2 for crystallization pressure of 193 MPa. Copolymer sample *i*PP4.38 exhibited the same behavior as *i*PP2.62, namely the γ-phase content increased with increasing crystallization temperature and pressure, however the WAXD patterns are not presented for brevity. In contrast with *i*PP2.62 copolymer *i*PP4.38 crystallized into pure γ-form even at the lowest crystallization pressure of 88 MPa, shown in Fig. 3.

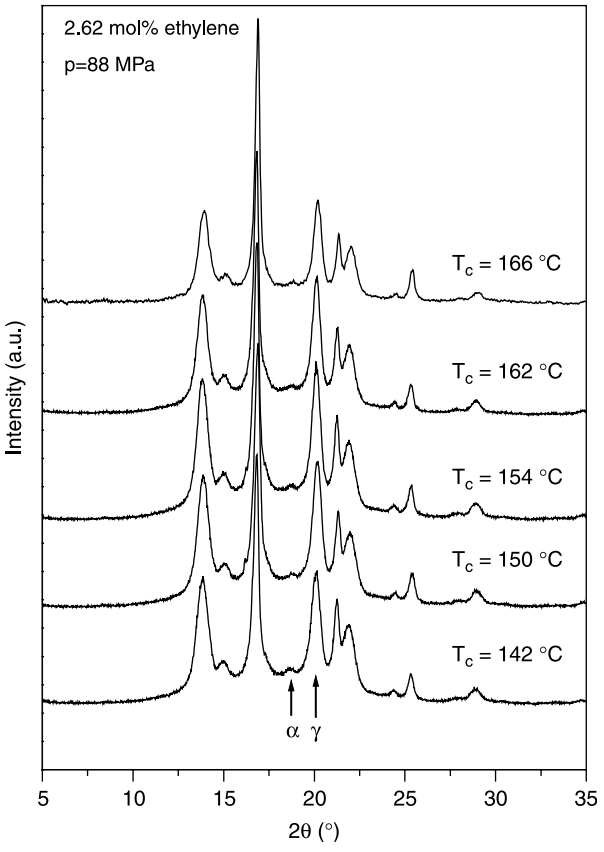

Fig. 1. WAXD patterns of *i*PP2.62 isothermally crystallized at 88 MPa.

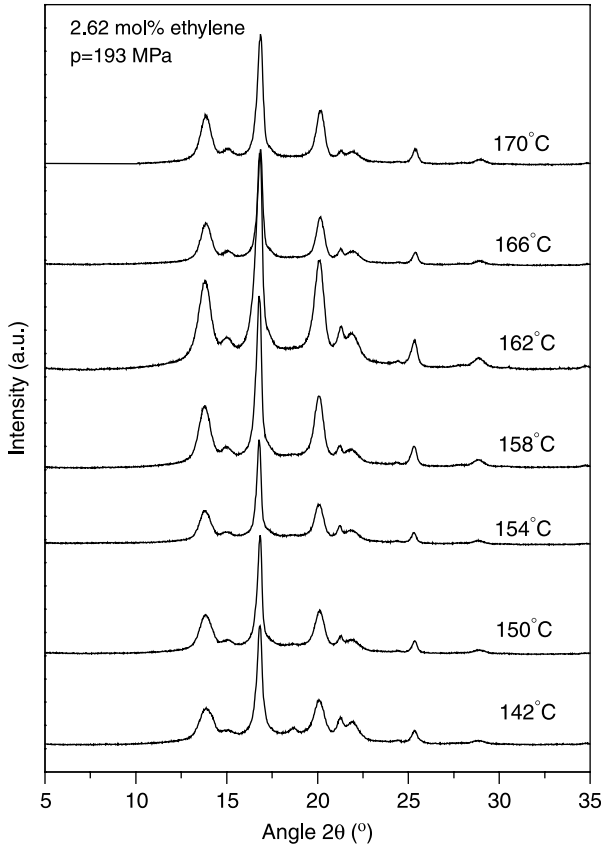

Fig. 2. WAXD patterns of *i*PP2.62 isothermally crystallized at 193 MPa.

3.2. DSC

Melting behavior of copolymer samples isothermally crystallized at high pressures was studied in DSC at atmospheric pressure. For all crystallization temperatures, melting endotherms exhibit one or two small peaks above the main melting peak. Figs. 4 and 5 show the melting endotherms of copolymer *i*PP2.62 crystallized at 88 and 193 MPa and different temperatures that correspond to the WAXD patterns in Figs. 1 and 2. Melting curves shown in Fig. 4 exhibit two endotherms, with the higher-temperature endotherm being much smaller than the lower-temperature endotherm. As expected, both peak temperatures increase with increasing crystallization temperature at constant pressure. Melting curves have a small 'hump' that appears at temperatures below their corresponding crystallization temperatures. As the crystallization temperature is increased the 'hump' becomes larger and better defined. The higher of the two small melting peaks that were observed in the melting curves of *i*PP2.62 crystallized at 193 MPa (Fig. 5, for crystallization temperatures of 142, 154 and 158 °C) was attributed to the melting-recrystallization-remelting phenomenon. This was confirmed by DSC analysis performed at different heating rates, which showed that the intensity of the highest melting peak decreases and even disappears with increasing heating rate.

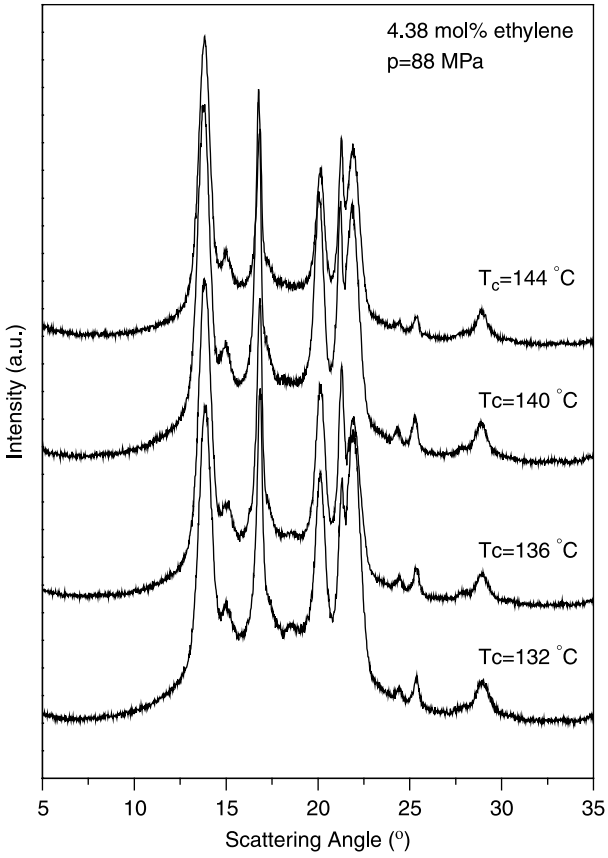

Fig. 3. WAXD patterns of *i*PP4.38 isothermally crystallized at 88 MPa.

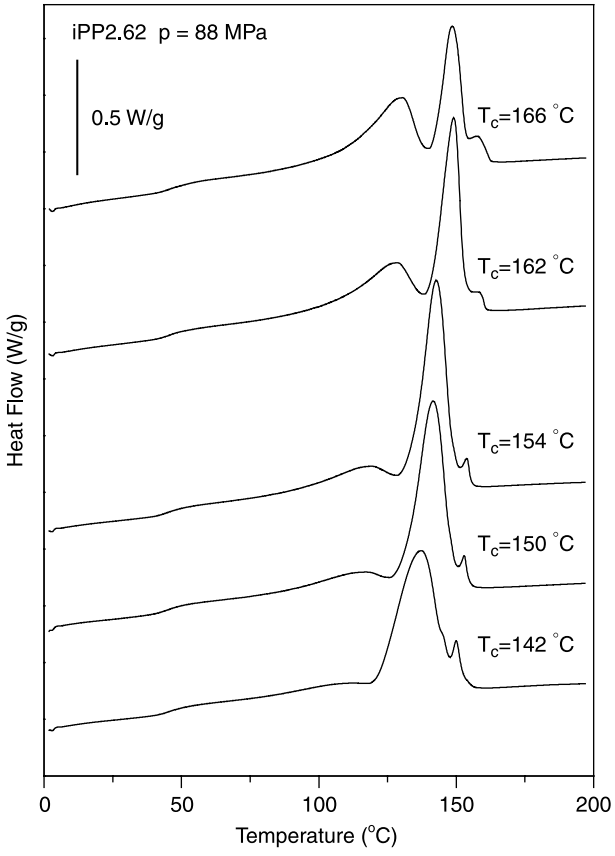

Fig. 4. DSC endotherms for *i*PP2.62 crystallized at 88 MPa as a function of isothermal crystallization temperature.

Consequently, these melting peaks were not used in the determination of the equilibrium melting temperature. WAXD analysis of the copolymer *i*PP2.62 crystallized at $p_c = 193$ MPa and temperatures above 162 °C detected 100% γ-phase, as seen in Fig. 2, while DSC scans show very small peak. Analysis of the peak area showed that the area of this peak is less than 1% of the total area. In contrast with copolymer *i*PP2.62, *i*PP4.38 samples crystallized at the highest crystallization temperatures and pressures did not exhibit the small melting peak above the main melting peak, as seen in Fig. 6.

4. Discussion

4.1. Formation of γ-phase

Crystallization of random propylene–ethylene copolymers at atmospheric pressure leads to the formation of a mixture of α- and γ-phase crystals. This has been reported for propylene copolymers synthesized with both Ziegler–Natta [23,24] and metallocene catalysts [17]. Results presented in Figs. 1–3 indicate that for the studied copolymers increasing crystallization pressure leads to an increase in the γ-phase content, and that at low degrees of supercooling pure γ-phase is obtained. Also, for the *i*PP4.38 copolymer with total defect content of 11.6 mol% pure γ-form was observed even at the lowest crystallization pressure. For this copolymer crystallization at pressures above 88 MPa and temperatures above 140 °C leads to pure γ-form regardless of the crystallization pressure. This can be observed more clearly in the plot of the γ-phase content as a function of crystallization pressure shown in Fig. 7(a) and (b). Therefore, increasing ethylene and total defect content shifts the onset of pure γ-phase formation in these propylene–ethylene copolymers to lower temperature values.

4.2. Equilibrium melting temperature of γ-phase of copolymers

Copolymers *i*PP2.62 and *i*PP4.38 that were crystallized at high pressures were analyzed in DSC at atmospheric pressure. Melting endotherms exhibited multiple melting, although less prominent than samples crystallized at atmospheric pressure [26]. For the *i*PP2.62 copolymer, all endotherms show a very small melting peak at a temperature above the main melting peak. Based on the peak assignment performed on the samples crystallized at atmospheric pressure using high temperature WAXD [26], the main melting peak was assigned to the melting of the γ-phase, and the small high-temperature melting peak to the melting of the α-phase. This is in agreement with peak assignments reported in the literature for both Ziegler–Natta and metallocene *i*-PP and propylene–ethylene copolymers [12,13,17,23,24]. The high-temperature peak is observed even for samples for which WAXD experiments did not show existence of the α-phase. A peak deconvolution was performed for all samples showing multiple melting endotherms, and the fraction of each melting peak was calculated. It was found, for

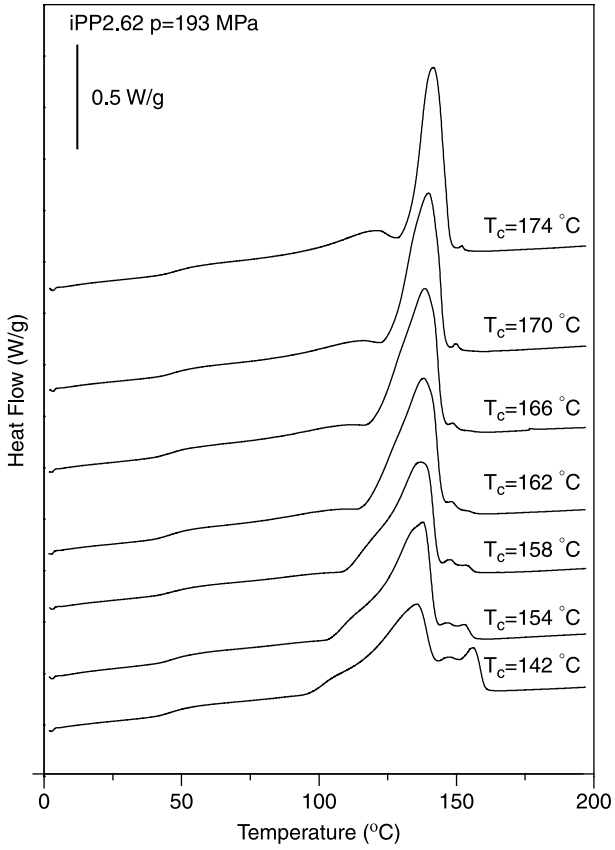

Fig. 5. DSC endotherms of *i*PP2.62 crystallized at 193 MPa as a function of isothermal crystallization temperature.

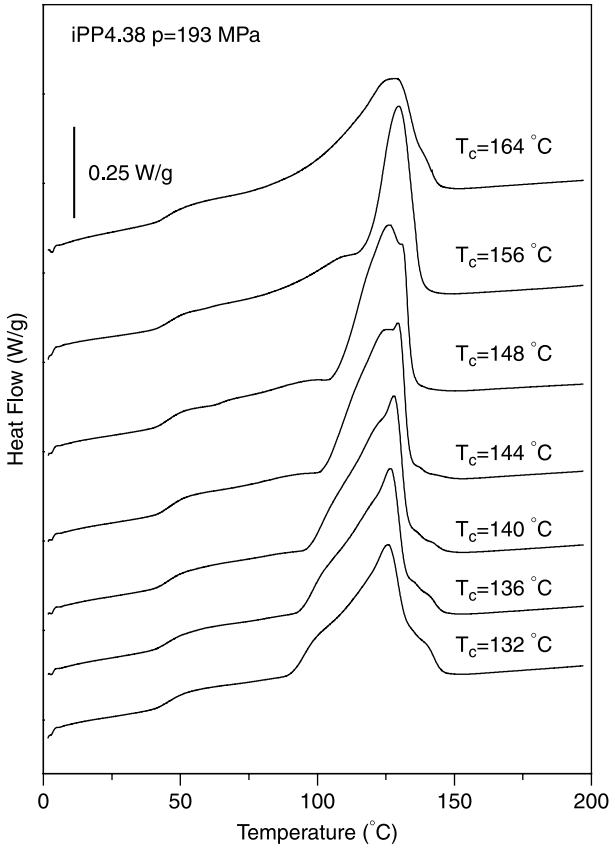

Fig. 6. DSC endotherms for *i*PP4.38 crystallized at 193 MPa as a function of isothermal crystallization temperature.

samples that did not show α-phase peak in WAXD, that the DSC α-peak is less than 1% of the overall peak area. We conclude that the DSC instrument is sensitive enough to register the melting of small quantities of α-phase crystals that are below the detecting threshold of the WAXD. On the other hand, the *i*PP4.38 copolymer samples crystallized at the lowest supercoolings at pressures of 158 and 193 MPa did not show any additional small endotherm above the main endotherm. This confirms well the results from WAXD analysis.

Samples crystallized at the highest temperatures regardless of the crystallization pressure exhibited broad melting endotherm at around 130 °C that increased in height with increasing crystallization temperature. This peak, in accordance with the results from the atmospheric crystallization [26], is due to the melting of thin crystals that are formed on quenching. The material that was not able to crystallize during the isothermal period of the crystallization crystallizes in the time frame when the crystallization temperature has been lowered to room temperature. In the high pressure experimental setup the maximum rate of cooling was 4–7 °C/min because of the bulkiness of the high pressure cell. This rate can not be considered as quenching, and some of the material will further crystallize during the cooling. Since the pressure was attained during the whole process of cooling to room temperature, there was no melting-recrystallization transformation from γ- to α-phase during the cooling.

In order to calculate the equilibrium melting temperatures (T_m^0) at different crystallization pressures the actual melting temperatures at the corresponding pressures are needed. DSC experiments from which melting temperatures were determined were performed at atmospheric pressure. To account for the change of melting temperature with pressure, all of the melting temperatures determined from DSC were corrected for the pressure. The correction was based on the experimental determination of the dependence of the melting temperature on the crystallization pressure by Zoller et al. [30] They have found that in the pressure range from 0 to 200 MPa the melting temperature of the *i*-PP increases by 0.285 °C/MPa. These experiments were performed on *i*-PP with high isotacticity (>96%) and molecular weight ~300 K.

Equilibrium melting temperatures of samples crystallized at high pressures were determined from Gibbs–Thompson plots of the melting temperature versus the inverse lamellar thickness. Peak temperature was chosen for the melting temperature, and for samples that had distinct α- and γ-phase melting peaks, attempts were made to use both temperatures for estimating the T_m^0 of α- and γ-phases as a function of crystallization pressure. Gibbs–Thompson plots for the γ-phase of the *i*PP2.62 and *i*PP4.38 are shown in Figs. 8 and 9, respectively. Equilibrium melting temperatures determined from Gibbs–Thompson plots for *i*PP2.62 copolymer γ-phase at 88, 123, 158 and 193 MPa are 203.4, 212.5, 220.2 and 229.6 °C, respectively. Equilibrium melting temperatures at the equivalent crystallization pressures

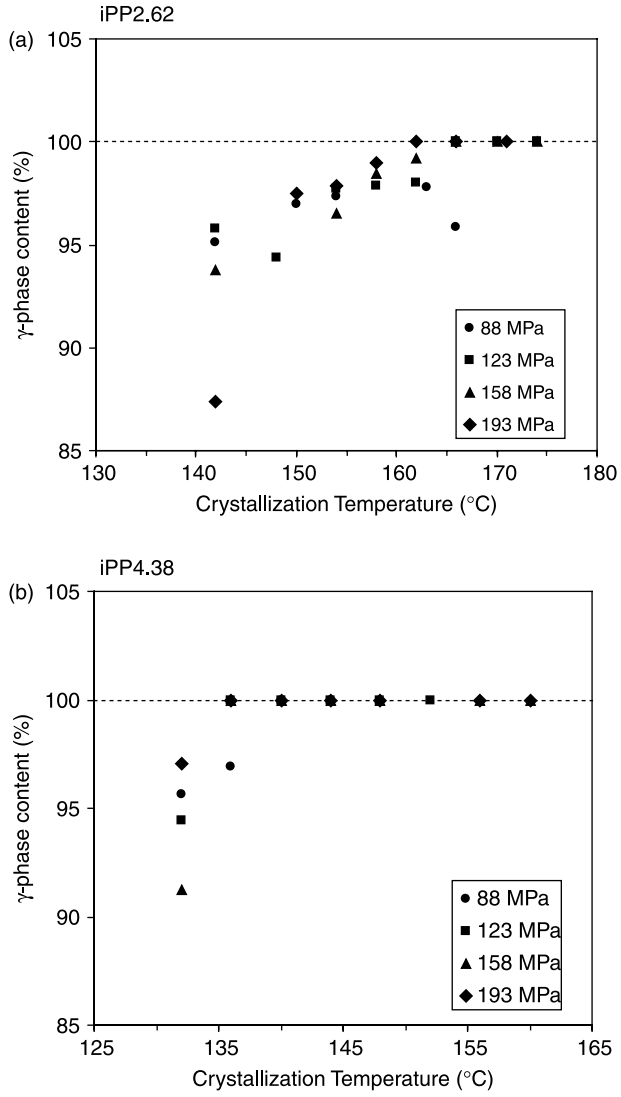

Fig. 7. Content of the γ-phase of (a) *i*PP2.62 and (b) *i*PP4.38 as a function of the crystallization temperature and pressure.

for γ-phase of *i*PP4.38 are 192, 198.4, 211.2 and 217.1 °C, respectively. It should be mentioned that for some of the curves in these plots there were only four experimental points available for extrapolation. Although this is regrettable, when crystallized at low pressures only a limited number of samples developed the pure γ-form so more experimental points could not be obtained.

Using the Gibbs–Thompson plot for calculating T_m^0 of the α-phase in the pressure crystallized samples would assume that both phases have the same average crystal thickness. SAXS Lorentz corrected data and 1D correlation function showed only one distribution of lamellar thicknesses. The content of the α-phase in these samples was very small, with the maximum amount of 5% detected in DSC measurements. In absence of more reliable data on the α-crystal thickness, a Hoffman–Weeks plot was used for determining the T_m^0 of the α-phase generated at elevated pressures. This plot for *i*PP2.62 samples is shown in Fig. 10, and obtained equilibrium melting temperatures at 88, 123, 158 and 193 MPa are 200.6, 209.0, 215.5 and 223.7 °C, respectively. In the case of the copolymer

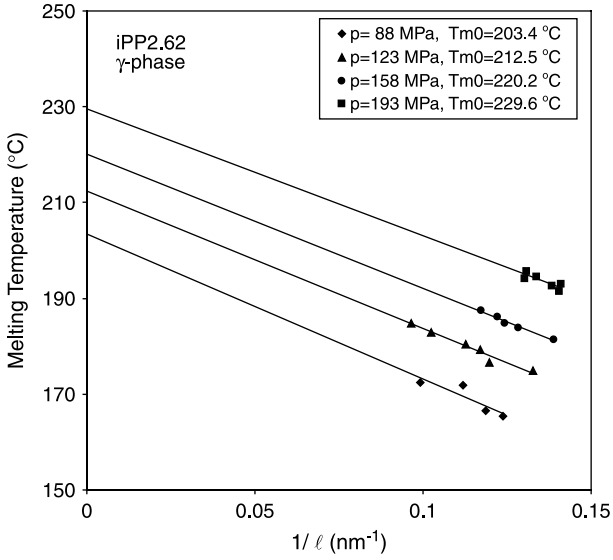

Fig. 8. Gibbs–Thompson plot of the melting temperature of γ-phase as a function of inverse lamellar thickness and crystallization pressure; sample *i*PP2.62 (total defect 5.76 mol%).

*i*PP4.38, there were not enough melting data points for the α-phase for a similar analysis to be performed.

Hoffman–Weeks plot of the *i*PP2.62 copolymer crystallized at $p = 153$ MPa, with extrapolations for both α- and γ-phases is shown in Fig. 11. It can be observed that the T_m^0 determined using the Hoffman–Weeks method (218.9 °C) is in good agreement with the T_m^0 determined from Gibbs–Thomson plot (220.2 °C). Similar results were observed for both copolymers crystallized at different pressures, where equilibrium melting temperatures determined from Hoffman–Weeks plots were always slightly lower. The differences in the T_m^0 stem from the different arguments on which these methods are based. Since Gibbs–Thomson method gives more accurate estimate of

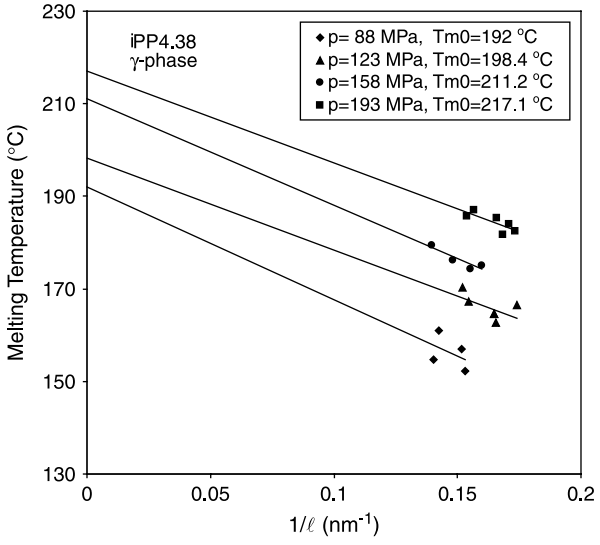

Fig. 9. Gibbs–Thompson plot of the melting temperature of γ-phase as a function of inverse lamellar thickness and crystallization pressure; sample *i*PP4.38 (total defect 11.60 mol%).

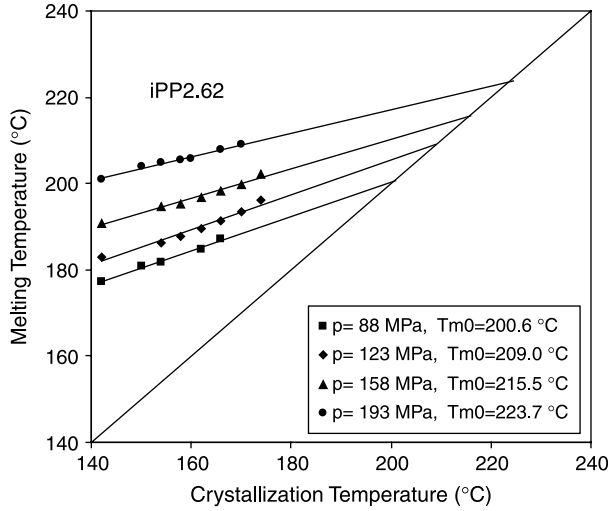

Fig. 10. Hoffman–Weeks plot of the melting temperature of α-phase as a function of crystallization temperature and pressure; sample *i*PP2.62 (total defect 5.76 mol%).

the equilibrium melting temperature, T_m^0 determined using this method will be further used in this study.

Another interesting observation seen on Fig. 11 is that although α-phase melts at higher temperatures compared with the γ-phase, when extrapolated to equilibrium conditions T_m^0 of α-phase is lower than that of the γ-phase. The slope of the extrapolation line for the γ-phase is always steeper than that of the α-phase, indicating that the thickening factor of the γ-phase is lower. Similar phenomenon has been observed for both *i*-PP[10] and propylene–ethylene copolymers crystallized at atmospheric pressure [26]. This behavior can be explained by the unique γ-orthorhombic crystal structure with non-parallel stem arrangement at 80°. This unorthodox chain arrangement can lead to formation of γ-crystals with little or no chain folding. The absence of chain folding or the presence of non-adjacent reentry of the copolymer molecules into the γ-crystals will cause a decrease in the lamellar thickening.

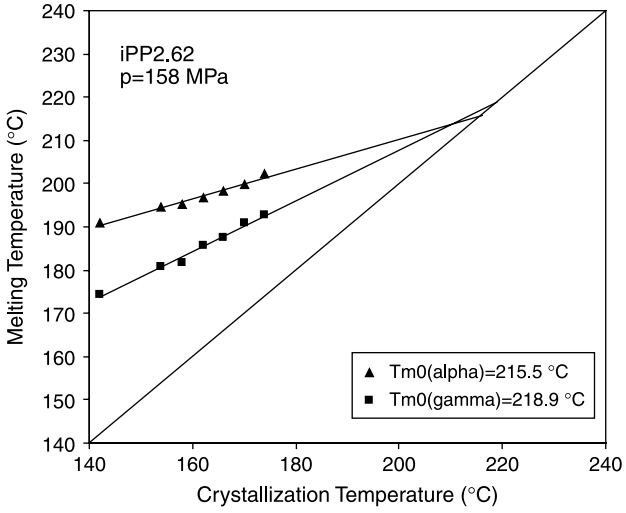

Fig. 11. Hoffman–Weeks plot for α- and γ- phases of *i*PP2.62 samples crystallized at $p = 158$ MPa.

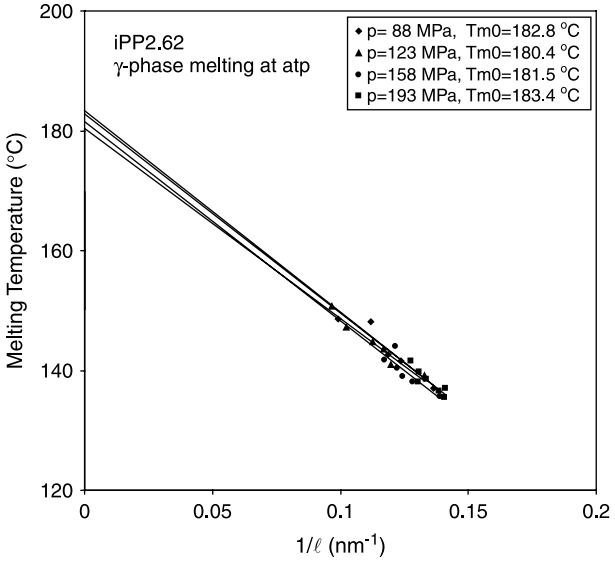

Fig. 12. Gibbs–Thompson plot of melting temperature recorded at atmospheric pressure of γ-phase as a function of inverse lamellar thickness; sample *i*PP2.62 (total defect 5.76 mol%).

T_m^0 of the copolymer γ-phase at atmospheric pressure could not be determined from the atmospheric crystallization studies, since pure γ-form could not be produced [26]. For that reason, T_m^0 of the copolymer γ-phase at atmospheric pressure was determined from high-pressure crystallized samples melted at atmospheric pressure. When melting temperatures of sample *i*PP2.62 not-corrected for the crystallization pressure are plotted on one plot (as shown in Fig. 12), they all extrapolate to 182 ± 1.5 °C. This temperature is the T_m^0 of γ-phase of the *i*PP2.62 copolymer at atmospheric pressure. Similar extrapolations for the *i*PP4.38 γ-phase are shown in Fig. 13, with the result being $T_m^0 = 170.7 \pm 1.7$ °C.

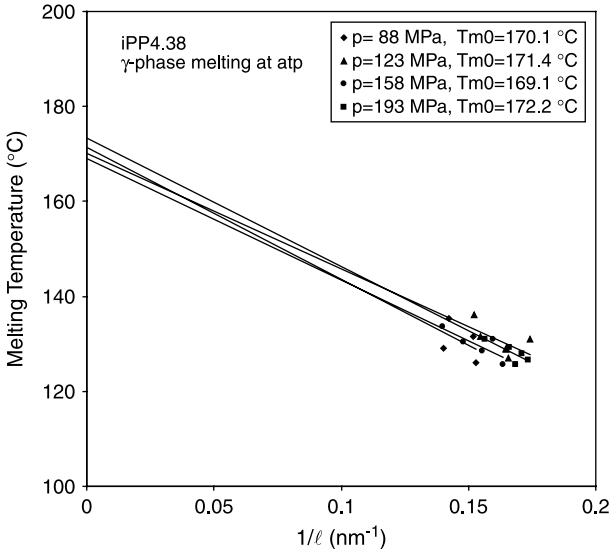

Fig. 13. Gibbs–Thompson plot of melting temperature recorded at atmospheric pressure of γ-phase as a function of inverse lamellar thickness; sample *i*PP4.38 (total defect 11.60 mol%).

4.3. Determination of heat of fusion (ΔH_f)

The pressure dependence of the equilibrium melting point can be used to calculate the heat of fusion of the polymer crystals through the application of the Clapeyron equation that defines the equilibrium between two phases:

$$\frac{dT_m^0}{dp} = \frac{T_m^0}{\Delta H_f}\left(\frac{\rho_c - \rho_a}{\rho_c \rho_a}\right) \quad (1)$$

where ρ_a and ρ_c are the melt and crystal densities (in g/cm^3), respectively, which are related to the specific volume changes from the crystalline to the amorphous state.

The plot of the T_m^0 versus the crystallization pressure of the γ- and α-phases for the *i*PP2.62 copolymer is shown in Fig. 14. These dependencies are linear, and the intercepts of the lines at $p_c = 0$ MPa are the T_m^0 of the α-phase determined from atmospheric pressure studies (172.6 °C) [26] and γ-phase (182 °C) determined from Fig. 12. Both sets of data in the plot can be represented with the Clapeyron equation, therefore the slopes of the lines are related to the heat of fusion and the density change (the right side of equation (1)). It should be mentioned that although the difference between the slopes of the two phases is small, the α-phase slope is slightly steeper. If γ-phase is favored at elevated pressure, the γ-phase slope should be larger than that of the α-phase. The higher value of the α-phase slope is due to the higher scatter of T_m^0 values, as seen in the Fig. 14, due to the limited number of experimental data available for extrapolation.

If the Clapeyron equation is valid, than ΔH_f does not change with the pressure and can be determined from the slope assuming that the densities also do not change with pressure. The value of the heat of fusion determined for the *i*PP2.62 α-phase is 165.0 J/g, and for the γ-phase 143 J/g. The value for the γ-phase is slightly lower than the value of 144.8 J/g [10] that was determined in a similar fashion for the homopolymer.

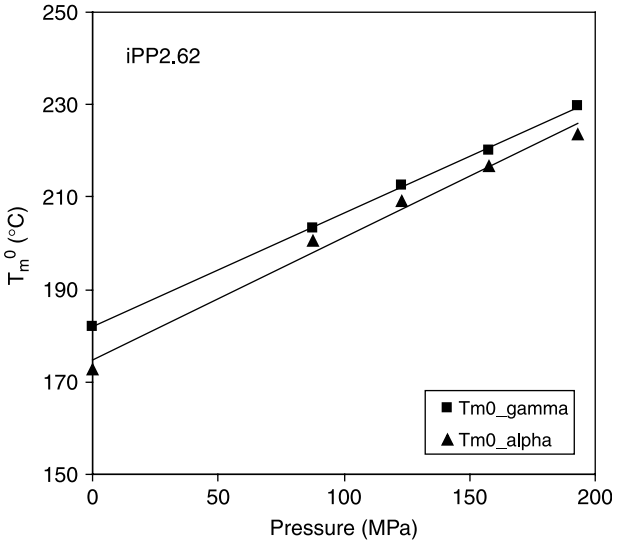

Fig. 14. Equilibrium melting temperature for α- and γ-phase as function of crystallization pressure; sample *i*PP2.62 (total defect 5.76 mol%).

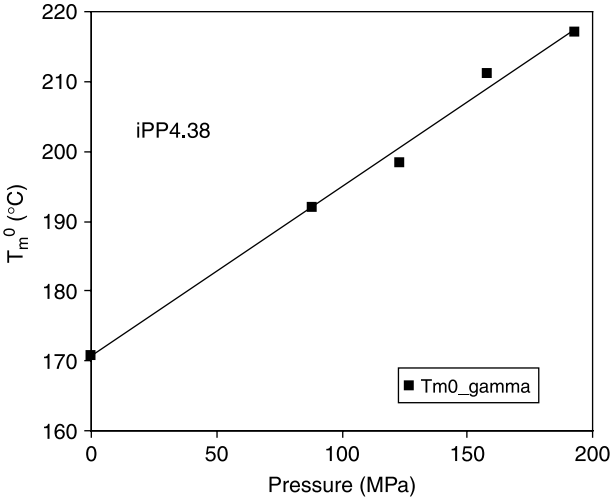

Fig. 15. Equilibrium melting temperature for the γ-phase as function of crystallization pressure; sample *i*PP4.38 (total defect 11.60 mol%).

Also, the value of 165 J/g is lower than the value of 167 J/g widely reported in the literature for the α-phase of the homopolymer. The equivalent plot of this dependence for the γ-phase of the *i*PP4.38 is presented in Fig. 15. Similar calculations were performed for the *i*PP4.38 copolymer samples, but in this case only for the γ-phase, because of the absence of the α-phase for most of the *i*PP4.38 samples crystallized at high pressures. The calculated value of the heat of fusion for the γ-phase of *i*PP4.38 was 141 J/g.

The reduction of the heat of fusion with increasing ethylene content has been reported for both unfractionated [24,31] and fractionated [25] Ziegler–Natta, as well as metallocene [32] propylene copolymers. These values for the heat of fusion are in a good agreement with the ΔH_f of the homopolymer reduced for the comonomer content.

An alternative method for determining the heat of fusion is based on the Clapeyron equation when the density changes with pressure. This method is very straightforward, and has been used to describe the melting behavior of many polymers [33,34]. All parameters that are needed for the calculation of the heat of fusion are obtainable from pressure-volume-temperature (PVT) data for the corresponding polymers, except for the crystal volume at the melting point. For this, data for the degree of crystallinity close to the melting point are needed. Since, no published PVT data for random low ethylene content propylene copolymers could be found, the PVT data for the *i*-PP homopolymer that have been published by Zoller et al. [30] were used. The previous homopolymer study [10] also used these PVT diagrams, and the same procedure will be followed here for consistent data treatment.

When the changes in the densities are estimated as a function of pressure from the PVT diagram, the heat of fusion of the copolymers can be calculated from the Clapeyron equation. Crystal densities of the copolymers were scaled down proportionally to account for the effect of the ethylene content on the copolymer density. The heat of fusion of the α- and γ- phase was determined as the best value that generated equilibrium melting temperatures similar to the experimental

Table 2
Thermodynamic parameters of α- and γ-crystalline forms for the *i*-PP homopolymer and the copolymers

Material	Phase	T_m^0 (°C)	ΔH_f (J/g)	ρ (g/cm^3)[a]
i-PP homopolymer[b]	α	186.1	209.0 167.0	0.936
	γ	187.2	190.0 150.0	0.933
*i*PP2.62	α	172.6	188.0 165.0	0.908
	γ	182.0	175.0 143.0	0.905
*i*PP4.38	α	165.7	170.0	0.899
	γ	170.7	164.0 141.0	0.896

[a] Density values were reduced to account for the effect of the ethylene content. Crystal density dependence on ethylene content was calculated from Hosoda et al. [32].
[b] Data from Ref. [10].

T_m^0. Table 2 lists the thermodynamic parameters of the α- and γ-crystalline forms for the copolymers and *i*-PP[10] obtained from the Clapeyron analysis.

Results of the Clapeyron analysis for copolymer *i*PP2.62 produced $\Delta H_{f,\alpha} = 188$ and $\Delta H_{f,\gamma} = 175$ J/g, while for *i*PP4.38 the value of $\Delta H_{f,\gamma}$ was 164 J/g. One can make an observation that analogous to the *i*-PP homopolymer, there are two different ΔH_f values for these copolymers depending on the method of evaluation. For example, these values for $\Delta H_{f,\gamma}$ are 190 and 150 J/g for the homopolymer, 175 and 143 J/g for *i*PP2.62, and 164 and 141 J/g for the *i*PP4.38 copolymer. For the copolymer *i*PP4.38 there were not enough experimental data to estimate the value of $\Delta H_{f,\alpha}$. However, for this purpose, based on the observed decreasing tendency of $\Delta H_{f,\alpha}$ a value of 170 J/g was suggested for the copolymer *i*PP4.38.

4.4. Temperature–pressure-composition phase diagram

One of the goals of this research was to append the existing *i*-PP α–γ phase diagram to include the effect of the composition on the thermodynamic stability of the phases. For this purpose, the stability of both phases as a function of temperature and pressure was evaluated. By performing the Gibbs free energy analysis in the study of *i*-PP[10] it was found that the pressure shifts the stability of the γ-phase to lower crystallization temperatures. It was predicted that at atmospheric pressure pure γ-phase is expected to form at a degree of supercooling of only ~10 °C, while the crystallization pressure of 200 MPa shifts this degree of supercooling to a much higher value of ~67 °C.

To calculate the ΔG for the copolymers two parameters, ΔH_f and T_m^0 of both phases, the latter as a function of crystallization pressure, are needed. As seen in Table 2, there are two values for the heat of fusion of α- and γ- phases depending on the defect content. The higher values were the ones determined from the Clapeyron equation in case of change of specific volume with pressure. These values will be used to calculate the Gibbs free energies of the phases. The equilibrium melting points of α- and γ- phases of *i*PP2.62 and γ-phase of *i*PP4.38 were determined from the high pressure experiments. The equilibrium melting temperatures of the *i*PP4.38 α-phase were calculated using the Clapeyron equation, and for 88, 123, 158 and 193 MPa these values are 188.4, 196.0, 203.8 and 211.2 °C, respectively.

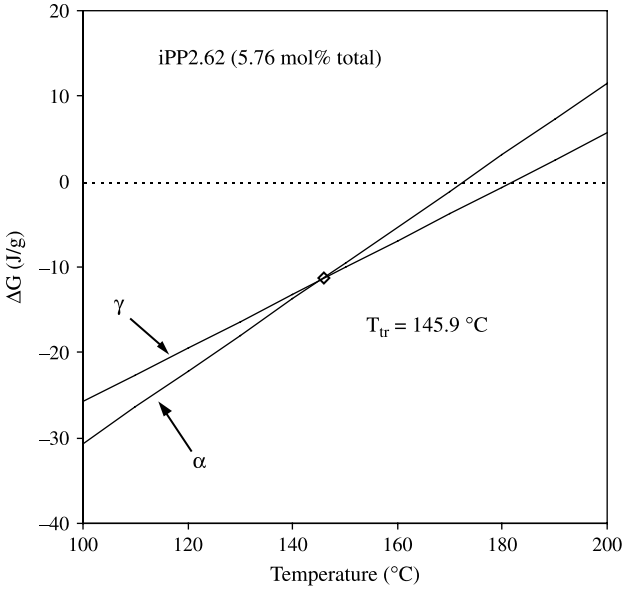

Fig. 16. Gibbs free energy diagram of α- and γ-phases as a function of temperature at atmospheric pressure, for *i*PP2.62 copolymer with 5.76 mol% total defect content.

Calculated Gibbs free energies of both phases as a function of temperature at atmospheric pressure are presented in Fig. 16 for sample *i*PP2.62 (5.76% tot.), and in Fig. 17 for the sample *i*PP4.38 (11.6% tot.). Corresponding plots for these samples at crystallization pressure of 193 MPa are shown in Figs. 18 and 19.

Values of the ΔG of both phases decrease with decreasing temperature, and the temperature at which these lines cross is the transition temperature at which the stability of the phases switches. From Figs. 16–19, it is observed that at temperatures

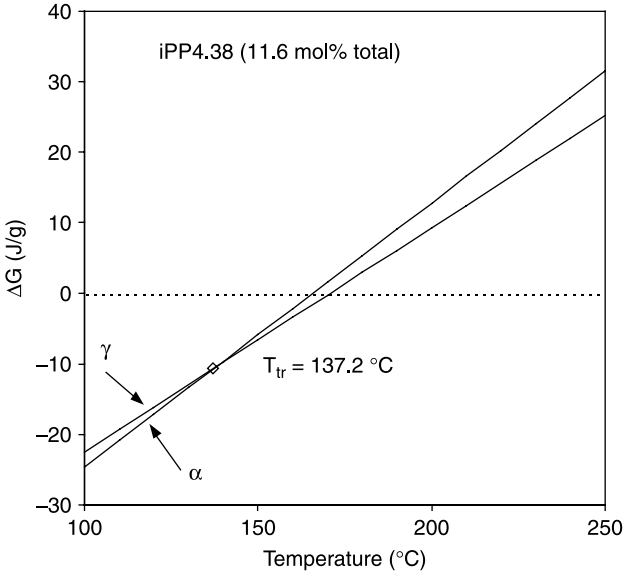

Fig. 17. Gibbs free energy diagram of α- and γ-phases as a function of temperature at atmospheric pressure, for *i*PP4.38 copolymer with 11.60 mol% total defect content.

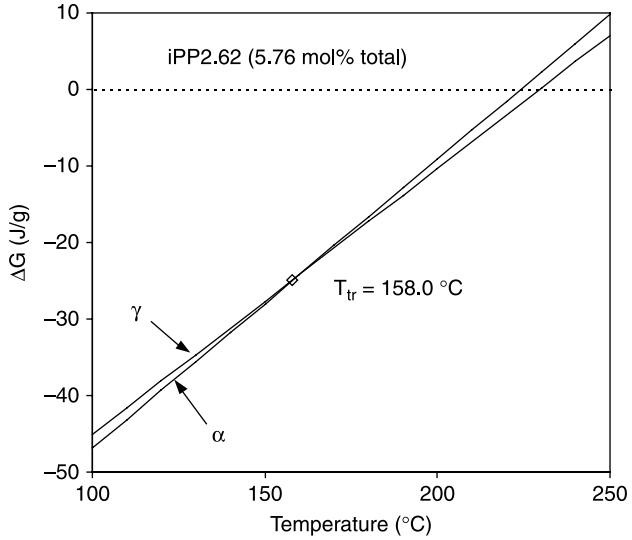

Fig. 18. Gibbs free energy diagram of α- and γ-phases as a function of temperature at 193 MPa, for *i*PP2.62 copolymer with 5.76 mol% total defect content.

below the transition temperature the more stable phase is α-phase, while above this temperature γ-phase is more stable. The transition temperature can be calculated from the equilibrium condition, by equating the free energies of both phases:

$$T_{tr}^{0} = \frac{T_{m,\alpha}^{0} T_{m,\gamma}^{0} \left(\Delta H_{f,\alpha} - \Delta H_{f,\gamma}\right)}{T_{m,\gamma}^{0} \Delta H_{f,\alpha} - T_{m,\alpha}^{0} \Delta H_{f,\gamma}} \tag{2}$$

Calculated transition temperatures for the atmospheric and $p_c = 193$ MPa are noted on the free energy diagrams. At atmospheric pressure 5.76 mol% defects decrease the transition temperature to 145.9 °C, while 11.6 mol% defects lower it to 137.2 °C. These values correspond to degrees of supercooling of 27 and 29 °C, correspondingly. Therefore, the degree of supercooling at which pure γ-form is expected to

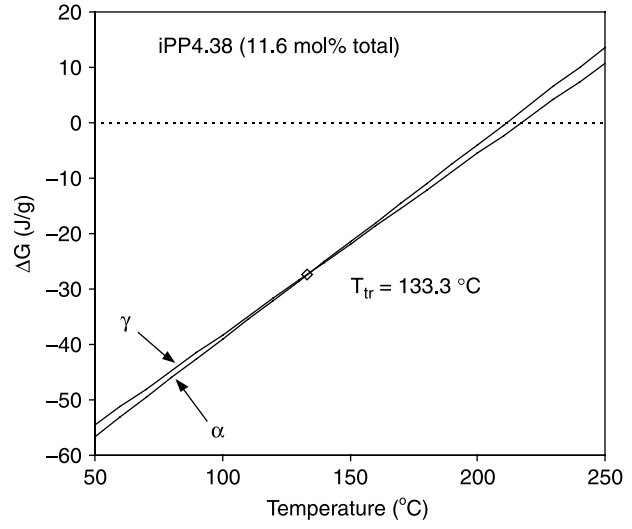

Fig. 19. Gibbs free energy diagram of α- and γ-phases as a function of temperature at 193 MPa, for *i*PP4.38 copolymer with 11.60 mol% total defect content.

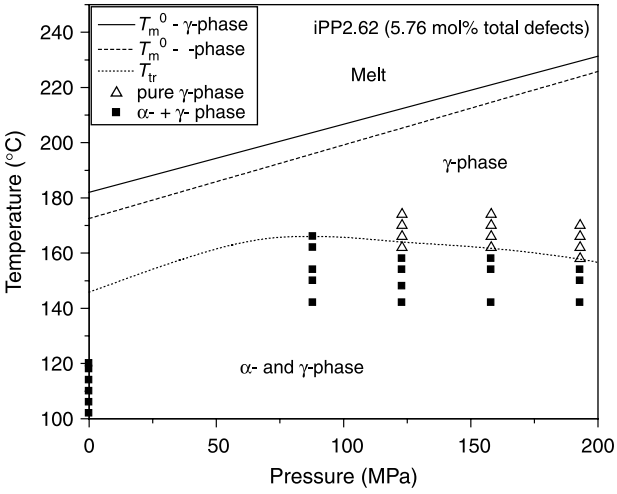

Fig. 20. Temperature–pressure phase diagram for copolymer with total defect content of 5.76 mol% (2.62 mol% ethylene).

form is increased from the 10 °C calculated for the *i*-PP homopolymer. The same tendency is observed at the highest crystallization pressure of 193 MPa. In this case, for copolymer with 5.76 mol% defects pure γ-phase is predicted to form at a degree of supercooling of 66 °C, while for copolymer with 11.6% defect this value is ~78 °C.

Using the T_m^0 of α- and γ- phases and calculated T_{tr}, temperature–pressure phase diagrams were constructed for both copolymer samples, shown in Figs. 20 and 21. On these diagrams lines define the regions of stability of both phases as a function of crystallization temperature and pressure, while scattered points are the experimental data. It can be observed that there is good agreement between the experimental points and the theoretical predictions. It should be noted that below the T_{tr} the more stable crystal phase is α-form, but all studied copolymers that were crystallized isothermally crystallized in a mixture of α- and γ-forms. Pure α-form was never observed in the studied crystallization temperature range.

Temperature–pressure phase diagrams of *i*-PP (1.26 mol% stereo defects), *i*PP2.62 (5.76 mol% total defect) and *i*PP4.38

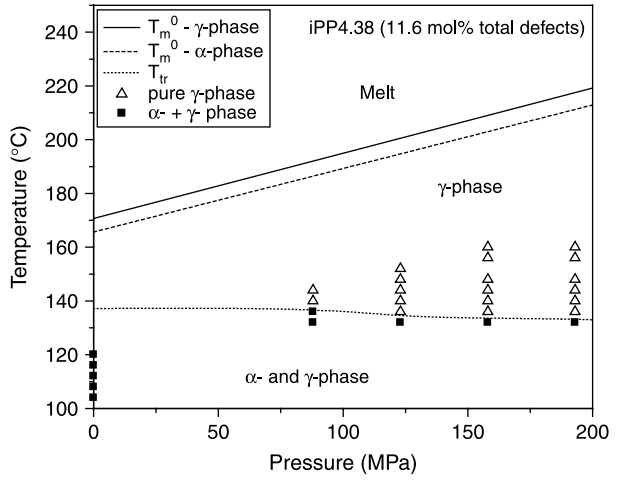

Fig. 21. Temperature–pressure phase diagram for copolymer with total defect content of 11.60 mol% (4.38 mol% ethylene).

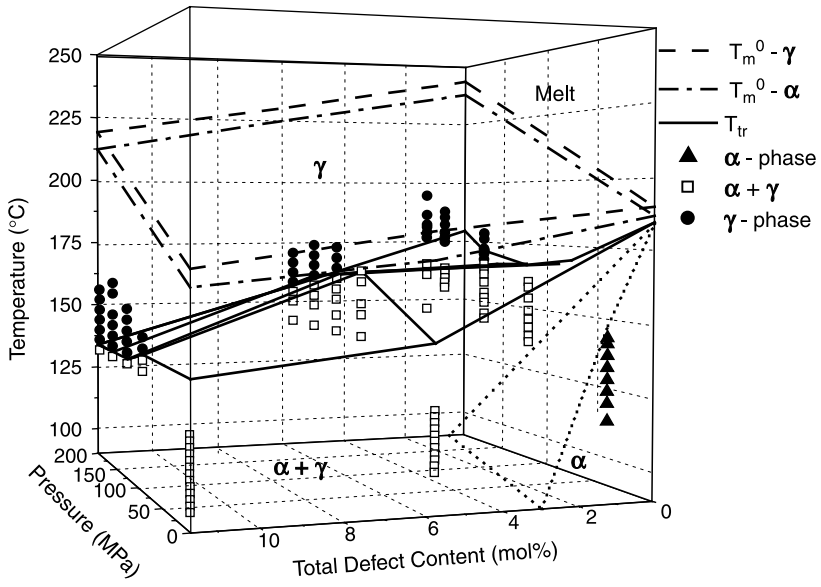

Fig. 22. Temperature–pressure-composition phase diagram for *i*-PP.

(11.6 mol% total defect) were used to construct the three dimensional (3D) phase diagram of *i*-PP with composition (total defect content) as an added third axis. The resulting 3D phase diagram is shown in Fig. 22, where the scattered points are the experimental data. The planes of the equilibrium melting temperatures of the γ- and α- phases are defined by the dashed and dot-dashed lines, correspondingly, while the solid lines outline the plane of the theoretical transition temperatures between the α- and γ-phases. These planes were extrapolated to zero defect content in order to evaluate the equilibrium parameters for defect-free *i*-PP, which are listed in Table 3.

From the results in Table 3 it can be observed that at atmospheric pressure the equilibrium melting temperature of the α- and γ-phase for defect free *i*-PP have higher values of 186.9 and 189.9 °C, respectively. Also, the transition temperature at which γ-phase becomes more stable than the α-phase increases to 184.7 °C, which is very close in value to the equilibrium melting temperature of the α-phase. Therefore, γ-phase of defect free *i*-PP cannot be expected to form on crystallization at atmospheric pressure.

5. Conclusions

Equilibrium melting temperatures of the α- and γ-phase of propylene–ethylene copolymers crystallized at high pressure were determined from SAXS, WAXD and DSC experiments using the Gibbs–Thompson and Hoffman–Weeks approaches. It was shown that T_m^0 of both phases decreases with increasing defect content. Analogous to the *i*-PP homopolymer crystallization, elevated pressures enhanced the formation of the γ-phase crystals. With increased crystallization pressure and temperature the concentration of γ-phase crystals increased for constant defect content. However, the presence of ethylene and stereo-defects in the copolymer chains greatly influenced the development of the pure γ-crystals. It was shown that increasing defect content shifts the onset of pure γ-phase formation in these propylene–ethylene copolymers to lower crystallization temperatures. Crystallization at pressures above 88 MPa and temperatures above 140 °C of copolymer with 11.6 mol% total defects led to pure γ-form regardless of the crystallization pressure.

Polymorphism and melting studies performed on the propylene–ethylene copolymers as a function of crystallization pressure enabled the modification of the existing α–γ phase diagram of *i*-PP homopolymer. Clapeyron equation and Gibbs free energy approach were used to evaluate the thermodynamic parameters of the α- and γ-crystal forms of the copolymers at atmospheric and high pressures. As a result, a temperature–pressure-composition phase diagram was constructed. *i*-PP homopolymer used in the original study was considered a stereo-copolymer with 1.26 mol% defects. This three-dimensional phase diagram enabled the extrapolation of the equilibrium melting temperatures of both phases, as well as the transition temperature, to zero defect content. Using this extrapolation method T_m^0 of the α-phase (186.9 °C) and γ-phase (189.9 °C) were obtained for defect free *i*-PP.

Table 3
T_m^0 of α- and γ-phases, and the T_{tr} between these phases for defect free *i*-PP obtained from Fig. 22

p (MPa)	$T_{m,\alpha}^0$ (°C)	$T_{m,\gamma}^0$ (°C)	T_{tr} (°C)
Atmospheric	186.9	189.9	184.7
75	206.1	209.9	169.7
125	218.8	222.9	166.6
175	231.6	235.8	171.2
200	238.0	243.7	179.2

Acknowledgements

This research has been supported by the National Science Foundation under grant DMR 0096505.

References

[1] Keith HD, Padden FJ, Walter NM, Wickoff HW. J Appl Phys 1959;30:1485.
[2] Natta GJ, Corradini P. Nuovo Cimento, Suppl 1960;15:40.
[3] Addink EJ, Beintema J. Polymer 1961;2:185.
[4] Turner-Jones A, Aizlewood JM, Beckett DR. Makromol Chem 1964;75:134.
[5] Bruckner S, Meille SV, Petraccone V, Pirozzi B. Prog Polym Sci 1991;16:361.
[6] Pae KD, Morrow DR, Sauer JA. Nature 1966;211:514.
[7] Kardos JL, Christiansen W, Baer E. J Polym Sci, Part A-2 1966;4:777.
[8] Campbell RA, Phillips PJ, Lin JS. Polymer 1993;34:4809.
[9] Mezghani K, Phillips PJ. Polymer 1997;38:5725.
[10] Mezghani K, Phillips PJ. Polymer 1998;39:3735.
[11] Morrow DR, Newman BA. J Appl Phys 1968;39:4944.
[12] Alamo RG, Kim MH, Galante MJ, Isasi JR, Mandelkern L. Macromolecules 1999;32:4050.
[13] Aurieamma F, De Rosa C. Macromolecules 2002;35:9057.
[14] Zimmermann HJ. J Macromol Sci, Phys 1993;B32:141.
[15] Mezghani K, Phillips PJ. Polymer 1995;36:2407.
[16] Laihonen S, Gedde UW, Werner PE, Martinez-Salazar J. Polymer 1997;38:361.
[17] Hosier IL, Alamo RG, Esteso P, Isasi JR, Mandelkern L. Macromolecules 2003;36:5623.
[18] Zhang J, Shen K, Na S, Fu Q. J Polym Sci: Part B: Polym Phys 2004;42:2385.
[19] Kardos JL, Christiansen W, Baer E. J Polym Sci, Part A-2 1966;4:777.
[20] Sauer JA, Pae KD. J Appl Phys 1968;39:4959.
[21] Morrow D. J Macromol Sci-Phys 1969;B3:53.
[22] Pae KD. J Polym Sci 1968;A-2:657.
[23] Marigo A, Marega C, Zannetti R. Makromol Chem 1989;190:2805.
[24] Busico V, Corradini P, Rosa C, Benedetto E. Eur Polym J 1985;21:239.
[25] Laihonen S, Gedde UW, Werner PE, Westdahl M, Jaaskelainen P, Martinez-Salazar J. Polymer 1997;38:371.
[26] Dimeska, A., PhD Dissertation, University of Tennessee, 2005.
[27] Turner-Jones A. Polymer 1971;12:487.
[28] Bruckner S, Meille SV. Nature 1989;340:455.
[29] Strobl GR, Schneider MJ. J Polym Sci, Polym Phys 1980;18:1361.
[30] Zoller P, Fakhreddine YA. Thermochim Acta 1994;238:397.
[31] Avella M, Martuscelli E, Volpe G. Makromol Chem 1986;187:1927.
[32] Hosoda S, Hori H, Yada K, Nakahara S, Tsuji M. Polymer 2002;43:7451.
[33] Starkweather HW, Zoller P, Jones GA, Vega AJ. J Polym Sci, Polym Phys Ed 1982;20:751.
[34] Starkweather HW, Zoller P, Jones GA. J Polym Sci, Polym Phys Ed 1983;21:256.